THE JOURNAL OF BIOLOGICAL CHEMISTRY VOL. 289, NO. 38, pp. 26514–26524, September 19, 2014

Dynamics of the Heme-binding Bacterial Gas-sensing Dissimilative Nitrate Respiration Regulator (DNR) and Activation Barriers for Ligand Binding and Escape*

Received for publication, April 8, 2014, and in revised form, July 8, 2014 Published, JBC Papers in Press, July 18, 2014, DOI 10.1074/jbc.M114.571398

Laura Lobato[‡§1], **Latifa Bouzhir-Sima**[‡§], **Taku Yamashita**[¶], **Michael T. Wilson**[‖], **Marten H. Vos**[‡§2], **and Ursula Liebl**[‡§3]

From the [‡]*Laboratory for Optics and Biosciences, CNRS, Ecole Polytechnique, 91128 Palaiseau, France,* [§]*INSERM U696, 91128 Palaiseau, France, the* [¶]*Laboratory of Analytical Chemistry, Graduate School of Pharmaceutical Sciences, Osaka University, Yamadaoka, Suita, Osaka 565-0871, Japan, and the* [‖]*School of Biological Sciences, University of Essex, Wivenhoe Park, Colchester C04 3SQ, United Kingdom*

Background: DNR is a recently discovered transcriptional regulator homologous to the CO sensor CooA.
Results: NO binding to heme selectively allows activation; ligand dynamics energetics implies common mechanism for 6-coordinate heme proteins.
Conclusion: DNR is an NO sensor acting as ligand trap.
Significance: Demonstration of NO-sensing function helps unravel signaling in the pathogen *P. aeruginosa* and describes common mechanism in emerging class of 6-coordinate heme proteins.

DNR (dissimilative nitrate respiration regulator) is a heme-binding transcription factor that is involved in the regulation of denitrification in *Pseudomonas aeruginosa*. In the ferrous deoxy state, the heme is 6-coordinate; external NO and CO can replace an internal ligand. Using fluorescence anisotropy, we show that high-affinity sequence-specific DNA binding occurs only when the heme is nitrosylated, consistent with the proposed function of DNR as NO sensor and transcriptional activator. This role is moreover supported by the NO "trapping" properties revealed by ultrafast spectroscopy that are similar to those of other heme-based NO sensor proteins. Dissociated CO-heme pairs rebind in an essentially barrierless way. This process competes with migration out of the heme pocket. The latter process is thermally activated (E_a ~7 kJ/mol). This result is compared with other heme proteins, including the homologous CO sensor/transcription factor CooA, variants of the 5-coordinate mycobacterial sensor DosT and the electron transfer protein cytochrome *c*. This comparison indicates that thermal activation of ligand escape from the heme pocket is specific for systems where an external ligand replaces an internal one. The origin of this finding and possible implications are discussed.

Bacterial heme-based gas sensor proteins allow for adaptation to different environmental stimuli, which is crucial for survival of the organisms (1–3). Diatomic gas signaling molecules such as O_2, CO, or NO are selectively sensed by a heme prosthetic group, and signaling is initiated by structural perturbation following formation or dissociation of the heme-ligand bond. Subsequently, intramolecular signal transmission events and long range structural changes take place to regulate physiological functions, including phosphorylation or DNA binding. Sensor proteins can contain heme in different coordination states when unliganded: in 5-coordinate heme-based sensors, an external effector molecule typically binds at the vacant distal position, whereas in 6-coordinate systems, an internal amino acid residue gets displaced in competition with an external gas molecule. These different sensing modes regulate ligand specificity and eventually determine downstream signaling events.

A recently identified addition to the group of 6-coordinate heme gas sensor proteins is DNR ("dissimilative nitrate respiration regulator"). DNR is a member of the cAMP receptor protein/fumarate and nitrate reductase regulator family of transcriptional regulators and mediates NO-dependent induction of denitrification in the opportunistic pathogen *Pseudomonas aeruginosa* (4). Homodimeric DNR has been purified in its apo-form without a heme cofactor but is able to stoichiometrically bind hemin *in vitro* with high affinity (5, 6). The protein is structurally similar to the bacterial heme-based CO sensor protein CooA of the cAMP receptor protein/fumarate and nitrate reductase regulator family (7, 8), which binds CO cooperatively and uses a 6-coordinate heme to regulate the expression of genes required for CO-oxidative growth. For CooA, large conformational changes, including domain rearrangements, have been predicted between the inactive and the active, DNA-binding state (8–10). An *a priori* unexpected feature of the DNR structure is the position of the sensing domain, which is rotated by ~60° with regard to the inactive structure of CooA (11). It has therefore been suggested that DNR equally undergoes large conformational changes for DNA binding, although in a different manner from CooA (11). How precisely heme controls the NO-dependent response of DNR is not known. However, it is noteworthy that, whereas the ferrous deoxy complex is 6-coordinate, the ferrous heme-NO complex appears 5-coordinate (6), a ligation form that is also observed in other heme-based

* This work was supported by Agence National de la Recherche Grant ANR-09-PIRI-0019 (to M. H. V. and U. L.).
[1] Recipient of a two-year fellowship from "La Caixa," Spain.
[2] To whom correspondence may be addressed. Tel.: 33-1-69335066; Fax: 33-1-69335084; E-mail: marten.vos@polytechnique.edu.
[3] To whom correspondence may be addressed. Tel.: 33-1-69335048; Fax: 33-1-69335084; E-mail: ursula.liebl@polytechnique.edu.

NO sensing proteins, in particular in soluble guanylate cyclase (12).

Qualitatively, it has been demonstrated that the DNR-NO complex binds to a promoter sequence associated with a denitrification enzyme (6). One of the aims of the present study is to quantitatively investigate the DNA binding affinity of DNR using fluorescence anisotropy measurements and its dependence on the heme ligation state. Physiological ligand-sensitive DNA binding in the nanomolar affinity range was deduced.

The primary processes in heme-based sensor switching mechanisms concern ligand binding to and ligand dissociation from heme (10). Photodissociation of the heme-ligand bond and subsequent monitoring of the spectroscopic changes occurring upon heme ligation provide an exquisitely sensitive probe of the heme-iron environment and allow characterizing the intraprotein migration of these diatomic gaseous molecules. Analysis of the dynamics of ligand binding and escape provides information about the mechanistic implication of these diatomic gases in early signaling events and insight into how the pathway of the dissociated ligand is controlled by the protein environment. Consequently, characterization of these primary processes, which typically occur on the picosecond time scale, is essential for a complete understanding of the switching mechanism in these sensors. Here, we investigated the recombination kinetics of CO and NO to the heme in DNR using femtosecond transient absorption spectroscopy. We observe that CO recombination in DNR is multiexponential and occurs roughly on the same time scale as in CooA, but with markedly less efficiency. Near complete and very fast NO recombination, as in other NO-sensing proteins, provides further support for a role of DNR as physiological NO sensor.

In general, in heme proteins, after dissociation of the heme-ligand bond, the yield of escape is considerably higher for CO than for NO or O_2 (13). Studies of the heme-based, 6-coordinate sensor protein Dos from *Escherichia coli* (*E. coli* Dos) showed that ~60% of dissociated CO rebinds to the heme on a nanosecond time scale (14, 15). The observation that rebinding and escape occur with similar rates made this sensor a suitable model for studying the activation barriers involved in these processes and revealed that CO rebinding is essentially barrierless, whereas CO escape is thermally activated (15). As in *E. coli* Dos the external gaseous ligand replaces an internal heme ligand, the question arises whether the escape enthalpic barrier experienced is related to this ligand competition. To investigate this question, we studied intraprotein CO migration and binding barriers in the physiological temperature range in DNR and CooA, with both being systems where the external gaseous ligand replaces an internal amino acid ligand. Comparison with a variant of the mycobacterial 5-coordinate heme sensor DosT, where no ligand is bound in the heme pocket in the absence of external ligands (16) and a ligand-binding variant of the electron transfer protein cytochrome *c* (17), which has no sensing role, indicates that CO rebinding from the heme pocket is a near-barrierless process and shines light on the factors determining the enthalpy barrier for ligand escape from the heme pocket.

EXPERIMENTAL PROCEDURES

Protein Expression and Purification—The *dnr* gene (4) from *P. aeruginosa* (684 bp) was subcloned into a pET-28a(+) vector (Novagen) using NdeI and BamH I restriction sites in frame with an N-terminal His_6 sequence. The construct was confirmed by sequencing and transformed into *E. coli* strain BL21(DE3). Transformants were grown in Luria Bertani medium containing 50 μg/ml kanamycin and protein expression was induced with 1 mM isopropyl 1-thio-β-D-galactopyranoside. For protein extraction, the cell pellet was resuspended in lysis buffer (300 mM NaCl, 50 mM NaH_2PO_4, pH 8.0, 5 μg/ml DNase, 1 mg/ml lysozyme) followed by sonication. The His_6-tagged polypeptide was purified using immobilized metal ion affinity chromatography columns (Protino Ni-TED, Macherey-Nagel) and eluted in 50 mM NaH_2PO_4, 300 mM NaCl, 250 mM imidazole, pH 8.0, followed by imidazole elimination on a Sephadex G-25 gel column (Sigma-Aldrich). For heme reconstitution, 100 μM purified DNR apoprotein (in 50 mM NaH_2PO_4, pH 8.0, 300 mM NaCl) and 400 μM ferric hemin (in 10 mM NaOH) were incubated 2 h at room temperature. Excess of hemin was subsequently removed on an Econo-Pac 10 DG gravity flow column (Bio-Rad).

CooA from *Rhodospirillum rubrum* was expressed and purified as described (18) and suspended in 100 mM Tris, pH 8.0. The wild type and Y169F mutant heme domains of DosT from *Mycobacterium tuberculosis* were prepared as described (19) and suspended in 50 mM Tris, pH 7.6, 150 mM NaCl.

Horse heart cytochrome *c* was purchased from Sigma. Carboxymethylated cytochrome *c* was formed by the addition of neutralized bromoacetic acid to the CN complex of native ferricytochrome *c* at pH 7. In this way, the intrinsic heme ligand, Met-80, is displaced from coordination and becomes available for reaction. Short incubation, 1 h at 25 °C, leads to minimal chemical modification (17), limited to Met-80 and one other residue, probably Met-65. Cyanide was removed by dialysis. In the ferrous form, the protein undergoes a pH transition, pK 7.2, from a penta-coordinate form at low pH to a hexa-coordinate form at high pH 9, in which a lysine amino group coordinates to the heme iron. Both forms bind CO with high affinity, $K = 1.3\ 10^9\ M^{-1}$ at pH 5.9 and $K = 8\ 10^7\ M^{-1}$ at pH 9.2. The spectral properties of the CO adduct are pH independent in this range. The ligand-binding properties of the modified protein have been described previously by Wilson *et al.* (20). The final carboxymethylated cytochrome *c* complex was suspended in 20 mM Hepes, pH 8.0.

Fluorescence Anisotropy-based DNA-binding Assays—Fluorescence anisotropy-based DNA-binding assays with DNR were performed using 6.4 nM DNA. Purified DNR was suspended in 50 mM Tris-HCl, pH 7.6, and 100 mM NaCl at a heme concentration of 5 μM in a gastight 1 × 1 cm optical path length cell, degassed, and reduced with 0.5 mM dithionite to obtain ferrous deoxy-DNR. To obtain the nitrosyl and carbonmonoxy adducts, the deoxy form was equilibrated with 1–10% NO (formation of the 5-coordinate ferrous DNR-NO complex could be verified spectroscopically; ferric DNR can also bind NO (6)) or 100% CO in the gas phase, respectively.

A 26-mer of double stranded DNA, corresponding to a fragment of the *P. aeruginosa nor* promoter (5) and containing the putative binding site for DNR, was obtained by mixing equimolar amounts of the two complementary oligonucleotides 5′-GGAATCTTGATTGCCATCAAGCGGGT-3′ (forward) and 5′-ACCCGCTTGATGGCAATCAAGATTCC-3′ (reverse) (Eurogentec). The 5′-extremity of the forward oligonucleotide was labeled with Texas Red. The oligonucleotides were heated 3 min at 80 °C followed by slow cooling down to room temperature to allow complete annealing. The DNA concentration in the assays was 6.4 nM. DNA was degassed in a gastight vial and, for the experiments with liganded DNR, equilibrated with a 10% NO or 100% CO atmosphere. Reduced DNR-NO or DNR-CO complex was added stepwise using a gastight Hamilton syringe up to concentrations of 300 nM. This procedure avoids loss of ligand from the DNR hemes upon addition. Fluorescence anisotropy was measured following a procedure as described (21) in a Cary Eclipse fluorometer equipped with a manual polarization device, with an excitation beam centered at 590 nm and scanning the Texas red emission spectrum. Anisotropy data were fitted to a hyperbolic binding curve (Langmuir equation) to determine the binding constant (K_d). For comparison, binding assays for CooA were performed similar as described in Ref. 22, using two strands of complementary 26-mer oligonucleotides containing P_{cooF} (5′-ATAACTGTCATCTGGCCGACAGACGG-3′ and 5′-CCGTCTGTCGGCCAGATGACAGTTAT-3′) (Eurogentec), with the 5′-extremity of the forward oligonucleotide labeled with Atto-390, and as a control, using the above-described *nor* promoter fragment, similarly Atto-390 labeled. In these experiments, the excitation beam was centered at 390 nm, and the Atto-390 emission spectrum was scanned.

Ultrafast Spectroscopy and Data Analysis—For ultrafast spectroscopy experiments, the samples were prepared as described for the DNA binding assays, but at a heme concentration of ~40 μM, in 1-mm optical path length gastight cells. Experiments on the DNR-NO complex were performed in the absence or presence of unlabeled *nor* promoter at a stoichiometric amount (one double-stranded DNA per dimeric DNR complex).

Most multicolor femtosecond absorption experiments were performed as described (23) with a ~30-fs pump pulse centered at 565 nm and a <30-fs white light continuum probe pulse, at a repetition rate of 30 Hz. Full spectra of the test and reference beams were recorded using a combination of a polychromator and a CCD camera. The sample was maintained in a thermostatted sample holder that was continuously moved perpendicular to the beams to ensure sample renewal between shots. At temperatures below 10 °C, nitrogen gas was blown over the cell surfaces to avoid condensation.

Multicolor femtosecond absorption experiments on the DNR-NO complex were performed on a 500 kHz repetition rate setup as described (24) based on a Quantronix Integra-C Ti-Saph oscillator/amplifier system, with a pump pulse centered at 570 nm. In this system, both test and reference probe beams pass through the sample, which is rastered with a Lissajous scanner.

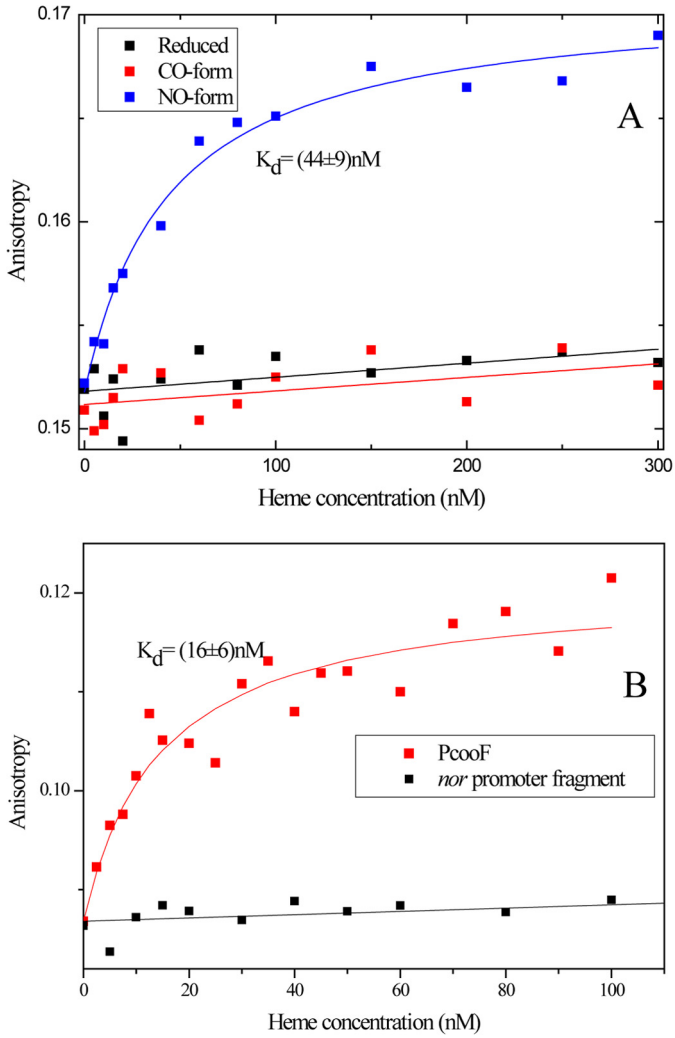

FIGURE 1. **Binding of DNR and CooA to labeled target DNA determined by fluorescence anisotropy.** *A*, high affinity binding of DNR to Texas Red-labeled *nor* promoter fragment target DNA is only observed in the NO-bound form and not with reduced or CO-bound DNR. *B*, binding of the CooA-CO complex to Atto-390-labeled target DNA (PcooF) and control reaction with Atto-390-labeled *nor* promoter fragment. The data of the latter are vertically displaced by −0.056 for clarity.

Correlated noise in the data sets was diminished by Singular Value Decomposition filtering. Data were globally analyzed in terms of multiexponential decay using the Glotaran package (25).

RESULTS

DNA Binding Affinity of DNR—As NO-dependent activation of DNR is thought to occur through a heme-induced conformational change (11), quantitative DNA-binding assays based on fluorescence anisotropy were carried out to determine the affinity of the transcriptional regulator DNR for *nor* promoter DNA in the active NO-bound form. Absorption spectroscopic analysis showed that NO was saturating under assay conditions. Addition of reduced DNR-NO to the labeled DNA increased the fluorescence anisotropy of the label, because formation of the DNR-DNA complex increases the volume of the labeled complex and hence slows down its rotational movement. From the saturation curve, a binding constant (K_d) of 44 ± 9 nM was determined (Fig. 1*A*). The reduced unliganded

and CO-bound forms of DNR exhibit almost constant anisotropy values and no saturation under the same conditions, consistent with low affinity and nonspecific DNA-binding.

We similarly determined the affinity of the CooA-CO complex for CooA-specific DNA at 16 ± 6 nM (Fig. 1*B*), consistent with the report of Ref. 22. As a control of specificity, a CooA binding assay was also performed under the same conditions using the *nor* promoter DNA. This assay did not result in observable specific anisotropy changes (Fig. 1*B*).

Ultrafast Recombination of NO in DNR—Due to the limited stability of the DNR-NO complex, ultrafast transient spectra can be obtained only with relatively poor signal to noise. Nevertheless, it is clear that photodissociation of the heme-NO bond in the 5-coordinate DNR-NO complex leads to formation of a 4-coordinate complex. After subpicosecond dynamics reflecting the heme photophysics, the transient spectrum (Fig. 2*A*, *inset*) is a typical 4-coordinate minus 5-coordinate nitrosyl spectrum (26–28). This spectrum subsequently decays in ~7 ps for >90% (Fig. 2*A*). These kinetics are similar to those obtained for the internal residue, suggesting that they reflect the intrinsic, barrierless bond formation between NO and heme. Heme-NO recombination generally has a very fast phase of 5–10 ps (13), but for most naturally ligand-binding proteins, additional phases and sizeable escape yield have been observed. A notable exception is the mammalian NO receptor GC (26), in which monophasic near unity QY recombination occurs.

In the presence of *nor* promoter DNA, the spectral evolution is identical within the signal/noise to what has been observed without target DNA (Fig. 2*A*), although the complex was significantly more stable in this case. This allowed us to determine that the decay phase amounts to >95% under these conditions.

Dynamics of CO in DNR and CooA—DNR has a predominantly 6-coordinate heme iron in the oxidized and reduced form (6), and binding of a gaseous signaling molecule will occur in competition with an internal amino acid residue ligand. Fig. 2 shows transient spectra at different delay times (*B*) and kinetics (*C*) after dissociation of CO from DNR. The transient spectra, with a minimum at 424 nm and a maximum at 442 nm, reflect the formation of a 5-coordinate heme upon CO dissociation. The shape of the transient spectrum remains virtually unchanged on the time scale of a few picoseconds to a few nanoseconds. This indicates that the spectral evolution reflects only CO rebinding to the heme and no formation of a 6-coordinate complex with two intrinsic residues. Upon dissociation, CO is located within the heme pocket, from which it can either rebind to the heme (geminate rebinding) or migrate out of the protein. The decay of the amplitude of the transient spectra implies that CO partially recombines on the picosecond-nanosecond time scale. The kinetics of rebinding are qualitatively similar to those of CooA (29, 30), but the amplitude of the recombination phase is much lower and as much as ~35% of the dissociated CO escapes the heme pocket. The rebinding kinetics can be well described by two exponential phases of ~100 (30%) and ~900 (35%) ps. These data indicate that in a substantial fraction of the proteins heme-CO recombination occurs on a similar time scale as CO escape from the heme pocket. Therefore, these kinetics are expected to be sensitive to

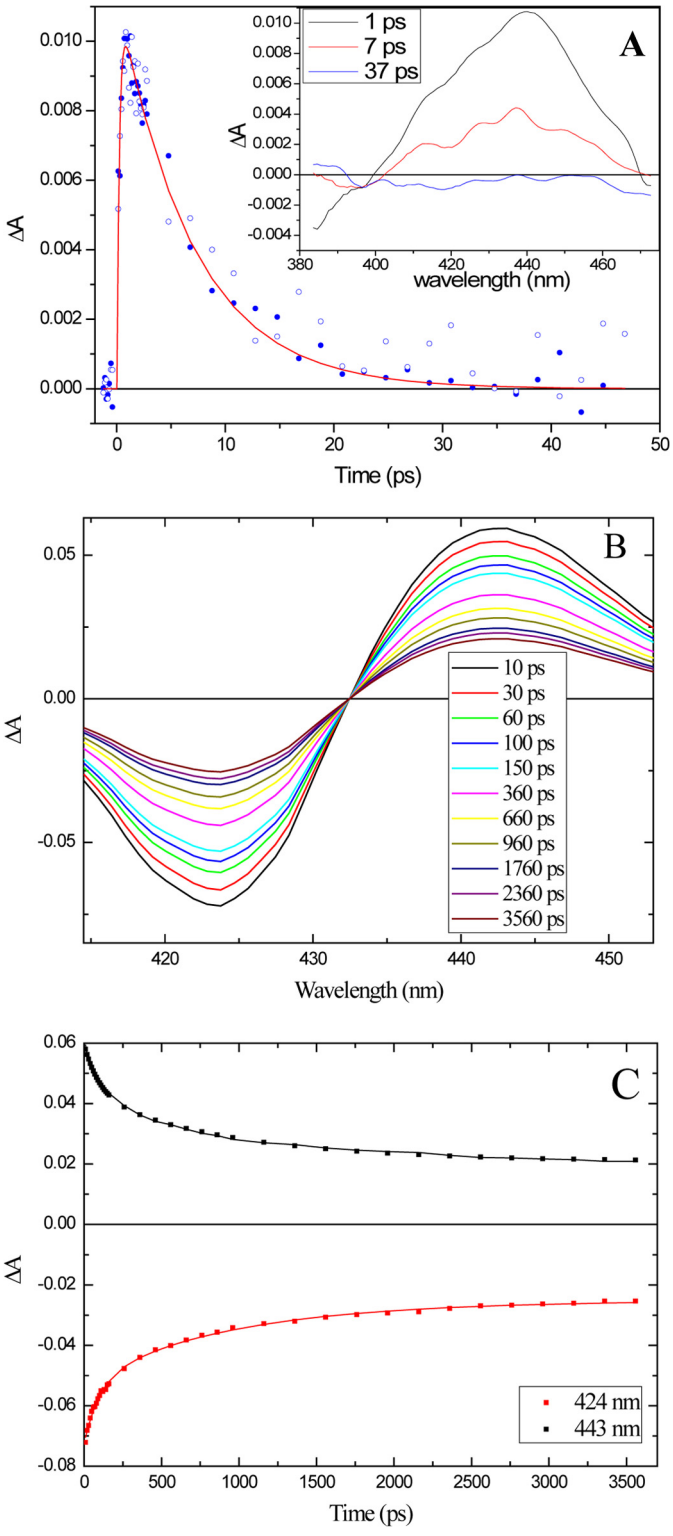

FIGURE 2. **NO and CO rebinding in DNR.** *A*, kinetics at 435 nm reflecting NO recombination to DNR in the absence (*open symbols*) and presence (*closed symbols*) of *nor* promoter DNA. The *solid line* is a fit to a single exponential with a time constant of 7 ps to the data with DNA resulting from a global analysis. *Inset*, transient spectra at different delay times in the presence of DNA. *Panels B* (transient spectra) and *C* (kinetics) reflect CO dissociation from and rebinding to DNR in buffer, at 20 °C. The *solid lines* in the kinetic traces are fits to two exponential components and a constant (see text) resulting from a global analysis.

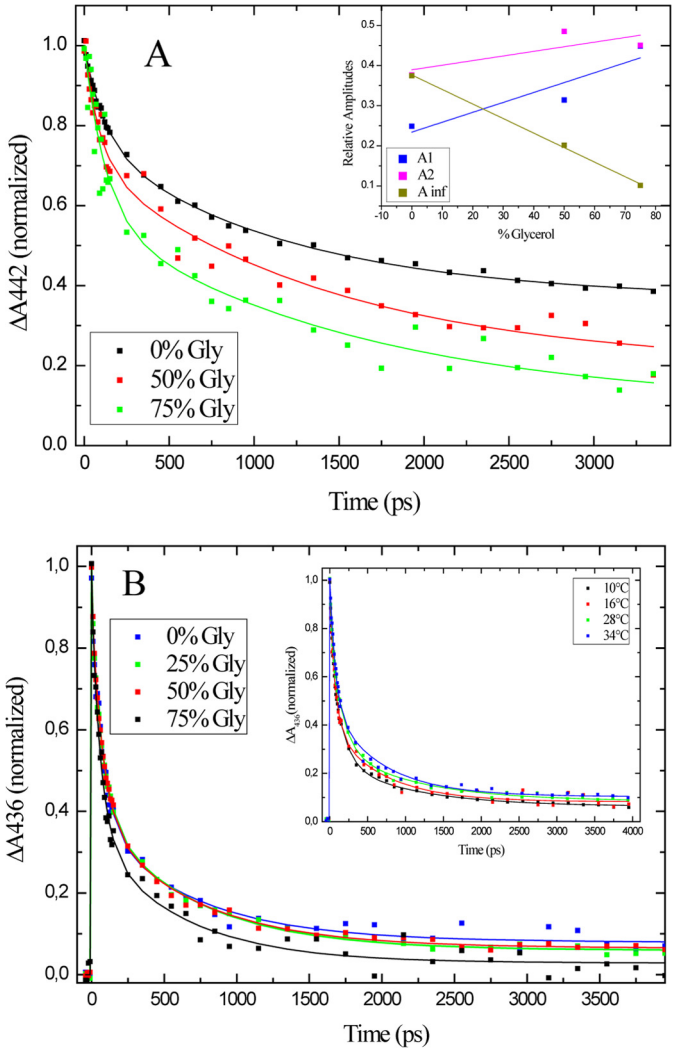

FIGURE 3. **Solvent viscosity dependence of CO rebinding.** Shown are the normalized kinetics of CO recombination at the induced absorption maximum in DNR (*A*) and CooA (*B*). The kinetics can all be fit with two decay components with similar time constants and an offset. The *inset* in *A* shows the amplitudes of the ~100-ps phase (A_1), the ~900-ps phase (A_2) and the offset (A_{inf}). The *inset* in *B* shows CO rebinding in CooA at different temperatures in the absence of glycerol.

parameters affecting the competition between CO escape and recombination to heme.

Fig. 3*A* shows that in DNR, upon increase of the solvent viscosity by adding glycerol, the escape yield of the dissociated CO strongly decreases. This effect is similar to what was previously observed for CO rebinding to *E. coli* Dos (15) and indicates that the solvent viscosity slows down protein motions that allow ligand escape, thus increasing the effective energy barrier for ligand escape. Interestingly, a qualitatively similar effect is observed for CO rebinding to CooA (Fig. 3*B*). As the ligand escape yield from the heme pocket is very low here (~5%), even in the absence of glycerol, the overall effect is much smaller than in DNR. Yet, these results indicate that barriers in ligand escape may also play a role in the multiphasic rebinding kinetics of CO to CooA (see below).

A more quantitative way to determine energetic barriers in ligand migration is to investigate the temperature dependence of the ligand dynamics. Fig. 4*A* shows the geminate rebinding kinetics of CO to the heme of DNR over a 24 ° temperature range. Clearly, at higher temperatures ligand binding decreases, indicating a significantly increasing CO escape yield. The amplitude and rate constant k_0 of the fastest decay phase (100 ps; (τ_1)) are constant within experimental error. All temperature dependence resides in the relative amplitude and rate constant of the slower phase (τ_2) (Fig. 4*B*). We therefore assign the fastest decay rate to a fraction α of dissociated CO that recombines directly with the heme in a barrierless way. The remaining, slower fraction β of dissociated CO can either rebind or escape. With the goal to gain insight into the direct competition between CO rebinding (k_1) and escape from the heme pocket (k_2), we analyzed fraction β according to the following Scheme 1 (see also Fig. 4*D*).

$$\mathrm{Fe-CO} \overset{k_1}{\longleftarrow} (\mathrm{Fe\ldots CO})_{\mathrm{I}} \overset{k_2}{\longrightarrow} (\mathrm{Fe\ldots\ldots CO})_{\mathrm{II}}$$

(Scheme 1)

Within this scheme, the observed rate constant k of CO rebinding to the bound state equals $k = k_1 + k_2$ and the rebinding fraction A equals $A = k_1/(k_1 + k_2)$ (31), so that we can relate the measured parameters k and A to the intrinsic rate constants k_1 and k_2 as $k_1 = Ak$ and $k_2 = (1 - A)k$ (15). Fig. 4*C* shows an Arrhenius plot of both rate constants k_1 and k_2. Whereas the rebinding reaction (rate constant k_1) is not activated ($E_a = 1 \pm 7$ meV), the escape reaction (rate constant k_2) experiences an activation barrier of ~70 meV (~7 kJ/mol) (Table 1). Altogether, we conclude that the temperature dependence of the CO rebinding kinetics can be essentially described by a barrier in CO escape, in agreement with the observed viscosity dependence.

A qualitatively similar temperature dependence of CO recombination is observed for the CO sensor protein CooA from *R. rubrum* (Fig. 3*B*, *inset*) and from *Carboxydothermus hydrogenoformans* (29). Unfortunately in CooA, a quantitative analysis similar to the one performed for DNR is complicated by the very low escape yield of CO. Together with our previous work on the 6-coordinate heme sensor protein Dos from *E. coli* (Table 1) (15), our findings indicate that in all these systems an enthalpy barrier for escape of the ligand from the heme pocket exists, whereas geminate rebinding to the heme, on the picosecond time scale, is not an activated process. Interestingly, in these three heme sensor systems studied, a functional exchange between an external diatomic ligand and an intrinsic ligand residue takes place. Therefore, a reorganization of the heme pocket must occur upon binding of an external ligand, possibly putting strain on the distal heme environment that may influence the ligand escape pathways and barriers. To further investigate this issue, we examined a heme sensor system in which sizeable CO recombination occurs within the heme pocket, but no exchange with an internal amino acid ligand takes place.

Dynamics of CO in DosT—The GAF A sensor domain of DosT from *M. tuberculosis* contains a heme that is 5-coordinate in the ferrous (Fe^{2+}) deoxy state (16, 32) and a distal tyrosine (Tyr-169) that interacts with heme-bound (33) and dissociated (19) ligands in the heme pocket. In wild type DosT,

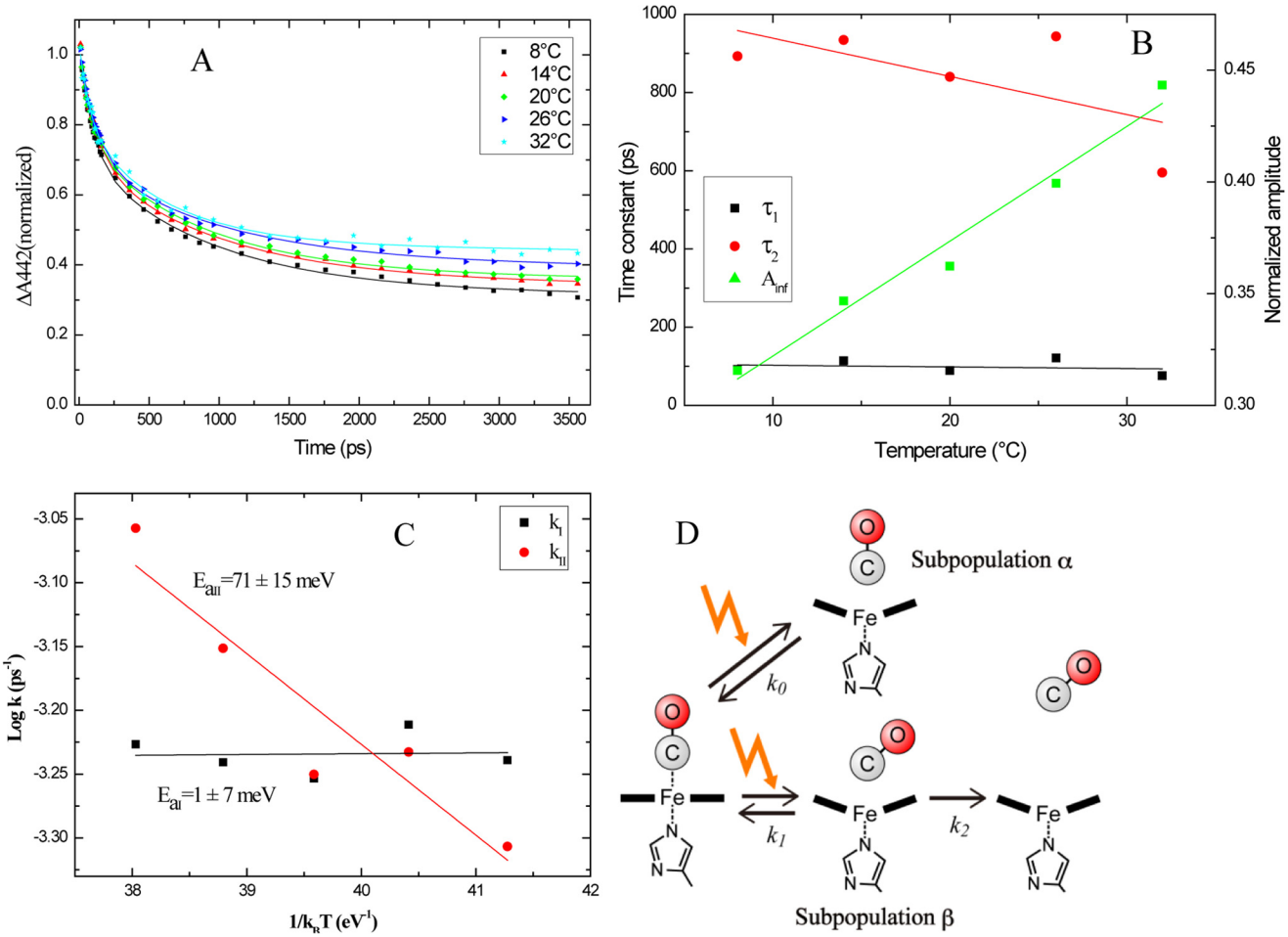

FIGURE 4. **Temperature dependence of CO recombination in DNR.** *A*, induced absorption kinetics at various temperatures. *B*, temperature dependence of the time constants of the decay phases and amplitude of the non-decaying fraction. τ_1, time constant of fastest decay phase; τ_2, time constant of slow decay phase; A_{inf}, amplitude of asymptotic phase. *C*, Arrhenius plot of the microscopic rate constants in DNR upon analysis according to Scheme 1. k_B, Boltzmann constant; *T*, temperature. *D*, scheme for the analysis of the T-dependent fraction of CO recombination to DNR. Two subpopulations with CO close to the heme are considered, being populated with different amplitudes immediately following CO dissociation. See text for details.

TABLE 1

Observed barriers for CO recombination and backward migration (E_b) and escape from the heme pocket and forward migration (E_f) in various heme proteins

Values are in meV.

	E_b	E_f	Ref.
DNR	1 ± 7	71 ± 15	This work
DosT Y169F	−9 ± 6, −1 ± 8	10.0 ± 20	This work
Carboxymethylated cytochrome *c*[a]	−18 ± 5, 11 ± 15	34 ± 9, 41 ± 9	This work
E. coli Dos	−4 ± 3	45 ± 10.0	Ref. 15

[a] See scheme in Fig. 6*C*.

CO-heme geminate recombination occurs to a modest extent (<20% up to 2 ns) and in a highly multiphasic way. This indicates that here CO escape from the heme pocket is more efficient than CO rebinding. We found that over the temperature range 10–28 °C, virtually no change in the CO rebinding kinetics occurs (data not shown). If the competition between rebinding and escape would be at the origin of the temperature dependence (as deduced for DNR and CooA), this finding might just be related to the low amplitude of the rebinding, rather than to barrierless ligand dynamics.

We therefore looked for a DosT variant susceptible to be more sensitive to changes in the balance of this competition. We found that substantially more extensive, as well as kinetically more homogeneous, recombination occurs in the DosT Y169F variant (19). Here, ~40% decay occurs with a major component in the 100-ps time range (19). Thus, in this mutant, escape and recombination rate constants are presumably more similar. Fig. 5*A* shows the CO rebinding kinetics at two different temperatures in this mutant. As in WT, the kinetics are very similar. To quantify eventual energy barriers, we performed an analysis similar to that of the DNR data.

Apart from a phase of a few picoseconds that has different spectral properties and can be ascribed to heme photophysics (19, 34), the spectral evolution can be described by two rebinding phases with time constants of ~70 ps and >~4 ns. The latter phase corresponds to a sizeable decay on the 2-ns time scale (Fig. 5*A*), but the amplitude and exact time constant of this phase cannot be determined within our time window. Based upon the analysis according to Scheme 1, we will assume that this phase reflects recombination from ligand positions out of the heme pocket ($(Fe.....CO)_{II}$ in Scheme 1); the relative amplitude of this phase (that includes all phases > 4 ns) then corresponds to the yield of escape from the heme pocket. Fig. 5*B* shows the relative amplitudes of the decay phases A_1 (~70 ps)

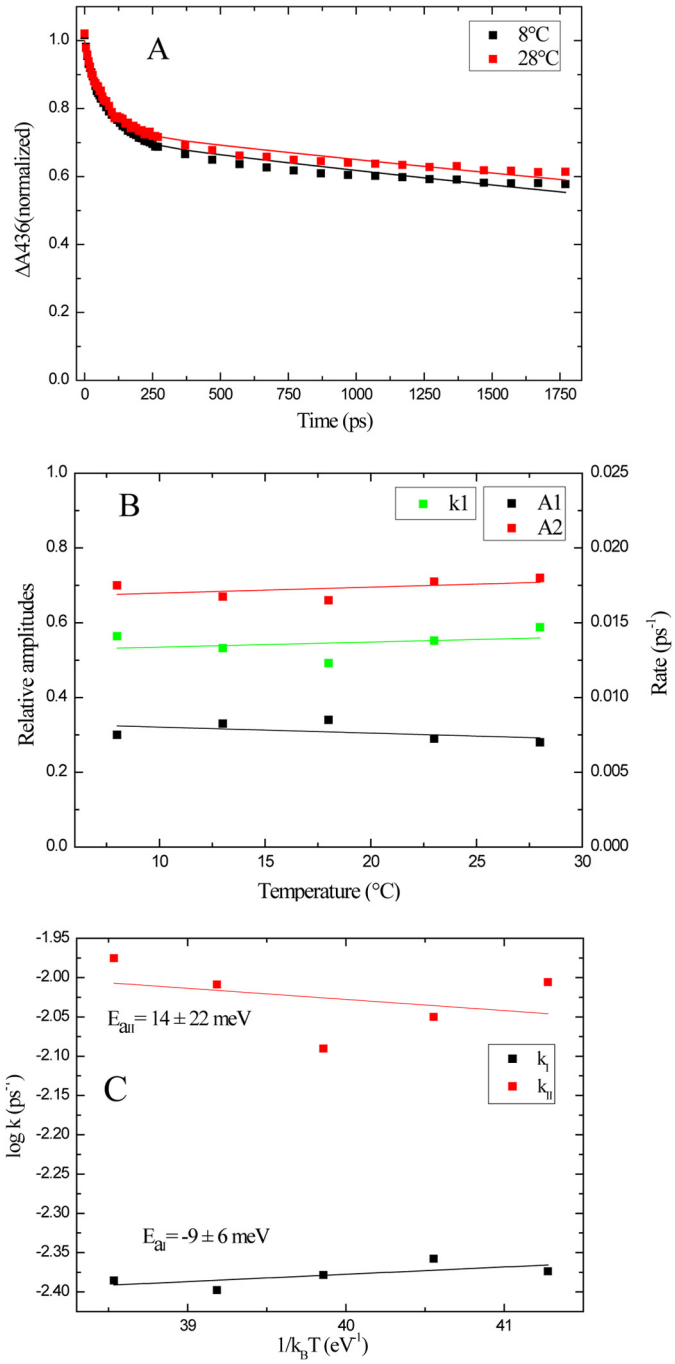

FIGURE 5. **Temperature dependence of CO recombination in DosT Y169F.** *A*, kinetics at 8 and 28 °C. *B*, temperature dependence of the rate constant of the picosecond phase and amplitude of the two decay phases. *C*, Arrhenius plots of the rate constants revealing that both processes are essentially barrierless.

and A_2 (>~4 ns) and the rate constant k_1 (of the picosecond phase) as a function of temperature. Both processes are found to be essentially barrierless (Fig. 5*C*). In particular, we deduce that the enthalpy barrier for ligand escape is <35 meV.

Dynamics of CO in Carboxymethylated Cytochrome c—To determine whether these observations are specific for heme sensor proteins, we compared these findings to a non-sensor heme protein. We therefore studied cytochrome *c*, the intrinsic function of which is not the interaction with external diatomic ligands, but electron transfer. Cytochrome *c* is a relatively rigid protein (35, 36) that is energetically optimized for its electron transfer function and the heme is 6-coordinate with histidine and methionine as axial ligands. Native cytochrome *c* does not readily bind external ligands, but in modified cytochrome *c* proteins, where the methionine ligand has been replaced or altered, CO (and other ligands) can coordinate to the heme cofactor (23, 37–41). In these systems, geminate heme-CO rebinding occurs on the picosecond-nanosecond time scale to an extent depending on the residue replacing methionine (23) or the chemical modification procedure (17). These systems are interesting models for ligand dynamics in intrinsically rigid protein systems. We choose to study carboxymethylated cytochrome *c* because it has both considerable CO rebinding and a substantial escape fraction (17) and is stable over a large temperature range.

Fig. 6*A* shows the CO recombination in carboxymethylated cytochrome *c* over the temperature range 10–75 °C. Here, the recombination is more heterogeneous than in the above-studied systems, as three exponential decays are required to fit the data (17), with time constants of ~10, ~100, and ~600 ps. Fig. 6*B* shows the relative amplitudes of the phases and of the non-decaying phase; the time constants do not strongly vary with temperature. As a minimal model to analyze the data, we assume that the fastest phase (~10 ps) arises from a distinct population that corresponds to direct barrierless recombination to the heme. The remaining four-parameter decay (comprising two exponential decay times and two independent amplitudes) was analyzed in terms of the simple four rate-constant model represented in Fig. 6*C* that is an extension of Scheme 1, including an additional intra-protein docking site. The resulting Arrhenius plots of this analysis are shown in Fig. 6*D*. Only the forward migration reactions (k_3 and k_5) are associated with significant (~40 meV) positive activation barriers. The back reactions do not significantly depend on temperature (k_1 and k_4) or even display a small negative barrier (k_2). The latter feature probably is not real and may reflect the fact that the model is an oversimplification and that additional states (either directly populated dissociated states or intermediate migration states) also play a role. Thus, qualitatively the overall trend in this protein is the same as in 6-coordinate heme-based sensor proteins and specifically the CO migration toward the exterior of the protein requires thermally activated protein motions.

DISCUSSION

DNA Binding Affinity of DNR—Fluorescence anisotropy-based DNA-binding assays were carried out to quantitatively determine the affinity of the transcriptional regulator DNR to *nor* promoter DNA in its active NO-bound and inactive forms. The non-saturating behavior of the reduced and CO-bound forms of DNR is consistent with some nonspecific binding, whereas for NO-bound DNR, the observed anisotropy saturation upon protein addition is a hallmark of sequence-specific, single site binding. The observed DNA binding constant (K_d) of 44 ± 9 nM and the high sequence specificity of binding are consistent with a transcription factor activity, although it is more than an order of magnitude lower than what is observed for active cAMP receptor protein (42). Our results provide direct evidence for NO-specific recruitment of DNR, in agreement with this transcription factor acting as NO sensor protein.

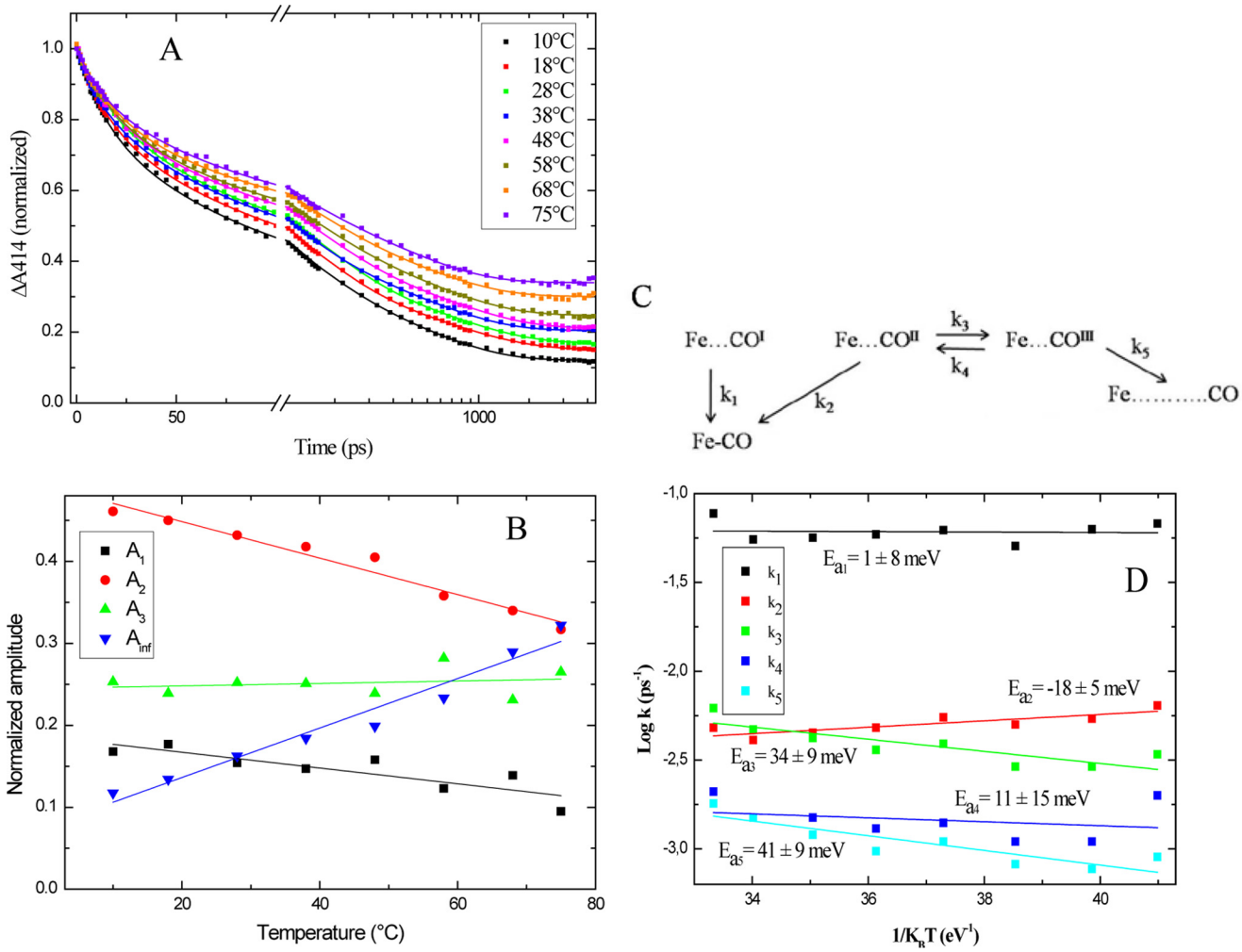

FIGURE 6. **Temperature dependence of CO recombination in carboxymethylated cytochrome *c*.** *A*, kinetics of negative absorption changes at various temperatures. *B*, temperature dependence of the relative amplitudes of the three decay phases (A_1, ~10 ps; A_2, ~100 ps; and A_3, ~600 ps) and of the non-decaying fraction (A_{inf}). *C*, reaction scheme for CO migration in carboxymethylated cytochrome *c*. *D*, Arrhenius plot of the microscopic rate constants upon analysis according to this scheme. k_B, Boltzmann constant; *T*, temperature.

Ligand Dynamics in DNR—Our data include the first ultrafast spectroscopic experiments on ligand dynamics in the presumed NO-sensing transcription factor DNR. Although the kinetics of CO rebinding to DNR occur on the same time scale as in the structurally related CO sensing transcription factor CooA, our data highlight that in DNR the yield of CO escape from the heme sensor pocket is ~10-fold higher. In DNR, recombination of NO takes place mono-exponentially and very efficiently (>90%) with a time constant of ~7 ps, similar as is observed in the mammalian NO receptor sGC (26, 43), suggesting this behavior to be a common feature in NO-specific heme sensors. Taken together these findings are in agreement with previous observations that heme sensor domains act as a trap specifically for the physiologically sensed ligand (10) and DNR acting indeed as NO sensor.

The only known structure of a 5-coordinate heme-NO complex is that of cytochrome *c′* from *Alcaligenes xylosoxidans* (44), where NO replaces the proximal histidine ligand. A similar equilibrium binding mode, reached via transient binding of NO on the distal side, has been proposed for sGC (45). The similar kinetic properties of NO rebinding to DNR (Fig. 2*A*), sGC (26) and cytochrome *c′* (28), might be considered as an indication of a similar binding mode in DNR. However, we note that the ligand binding mechanism must be different in DNR, as NO binding is associated with the dissociation of two internal heme ligands, whereas in sGC and cytochrome *c′*, the heme is five-coordinate in the deoxy state. For now, in the absence of structural information on the heme environment; these issues remain to be clarified.

Effect of DNA Binding on Ligand Recombination—Recent work by Champion and co-workers (29) has shown that binding of DNA to the CooA-CO complex leads to kinetically more homogeneous heme-CO rebinding, an observation that was interpreted in terms of DNA-induced stabilization of a specific protein configuration. For the DNR-NO complex, in the absence or presence of bound DNA, we observed identical, mono-exponential, kinetics within experimental error (Fig. 2*A*). As NO recombination in 5-coordinate complexes of heme-based sensors always occurs with high efficiency within a few picoseconds (10), the NO recombination kinetics are likely not very sensitive to protein configurational changes. We note, however, that our qualitative observation of higher complex

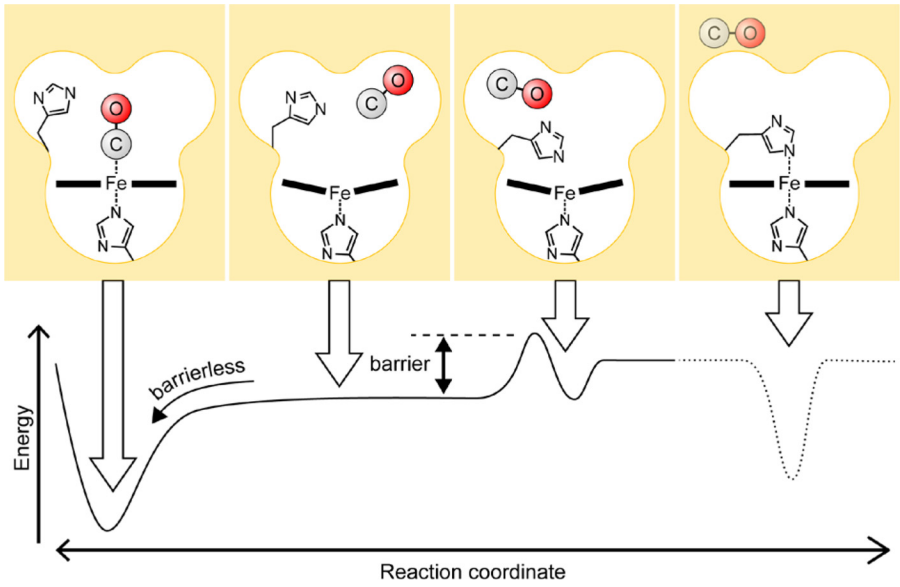

FIGURE 7. **CO escape and heme binding in 6-coordinate heme sensor proteins.** General energy (*bottom*) and configurational (*top*) schemes are shown. Here, the residue coordinating at the distal side is depicted as a histidine. The configuration on the *right*, corresponding to the heme with two protein axial bonds and CO in the environment, is not reached within the time scale of our experiments; consequently, the corresponding energy landscape is depicted with a *dotted line*.

stability upon DNA binding is consistent with conformational selection upon specific binding of DNA.

Activation Barriers for CO Escape and CO-heme Binding—We used CO recombination kinetics on the picosecond and nanosecond time scale to probe the energetic barriers of geminate CO rebinding and intraprotein migration in two 6-coordinate heme sensor proteins: *P. aeruginosa* DNR and *R. rubrum* CooA. Our findings were compared with the 5-coordinate mycobacterial, heme-based sensor DosT and the electron transfer protein derivative carboxymethylated cytochrome *c* (Table 1). All investigated heme proteins display substantial CO recombination on the picosecond and nanosecond time scale. This is in contrast to myoglobin and hemoglobin where the lack of recombination effectively competing with escape prohibits determination of the energetic parameters (although similar primary CO escape mechanisms may occur as in DosT).

Barrierless CO Recombination—We found that for all studied complexes: DNR, *R. rubrum* CooA, DosT, and carboxymethylated cytochrome *c*, as well as for the previously studied *E. coli* Dos (15), intrinsic heme-CO rebinding on the picosecond time scale takes place essentially without an enthalpy barrier. These findings are also in agreement with similar experiments in *C. hydrogenoformans* CooA, concluding no enthalpy barrier from the distal heme pocket (29). In the latter work, a modest temperature dependence was attributed to changes in the distribution of the heme configuration, whereas in the systems studied in our work, the temperature predominantly influences the ligand escape yield. The time constants of the barrierless rebinding processes range from ~10 ps to a few ns in these proteins and are mostly heterogeneous. This variation implies that these time constants do not represent the intrinsic time of bond formation between free CO and 5-coordinate domed heme. We propose that they correspond to the time that the dissociated ligand requires for sampling different configurations within the heme pocket, until it eventually finds a configuration allowing heme-ligand bond formation, reflecting the entropy contribution to the recombination process. Consequently, the variation in the binding time constants reflects different formation times of favorable binding configurations compared with the ensemble of possible configurations within the heme pocket. Thermal motions of the environment do not significantly influence these sampling rates, suggesting that they can be viewed as motions in a relatively immobile cage and that protein constituents do not form a physical barrier between ligand and heme. As CO binds to heme in a near-perpendicular configuration, the CO orientation with respect to the heme normal is expected to be a critical parameter. The barrierless binding rate constants deduced within several protein systems presumably reflect distinct heme-CO bound configurations that interconvert slowly on the time scale of the experiment as have been observed in time-resolved infrared experiments in CooA (46) and carboxymethylated cytochrome *c* (47).

Ligand Escape from the Heme Pocket—For the DNR-CO complex, our analysis indicates an energy barrier of ~70 meV for migration of CO from the initially dissociated configuration (from which direct recombination is possible) to a further lying configuration. This barrier is of the same order of magnitude as the one (45 meV) previously established for *E. coli* Dos (15). In CooA, qualitatively similar results were obtained, but the yield of escape was too low to allow a quantitative estimation of the enthalpy barrier. As indicated before, in these three six-coordinate heme sensor proteins an external ligand replaces an internal amino acid residue (Met for *E. coli* Dos (48), N-terminal Pro for CooA (7) and probably His for DNR (49)). In contrast, the enthalpy barrier for ligand escape in DosT, where the heme is 5-coordinate in the absence of external ligands, was zero within experimental error. This comparison suggests that the presence of a replaced internal ligand in 6-coordinate systems creates a barrier for ligand escape, a suggestion that is in general agreement with the notion that the replaced internal amino acid residue is constrained to undergo substantial reconfigura-

tion. Conversely, this internal ligand exerts, directly or indirectly, strain on the dissociated external ligand and, rather than forcing the ligand out of the near heme environment, creates a barrier for its escape. In this way, the barrier helps to "trap" the ligand in the heme pocket (10, 50). We emphasize that the protein motions allowing CO to escape are not directly involved in placing the internal ligand in a favorable binding condition within the heme pocket, as internal ligand rebinding upon CO dissociation occurs in microseconds and is negligible on the nanosecond time scale. Also, binding of CO (and NO) from solution to the 6-coordinate ferrous complex occurs on the 10^{-1}–10^{0} s time scale and is rate-limited by the dissociation of the internal residue ligand (6), as is also the case in CooA (51). Thus, whereas the barrier for ligand escape from the heme pocket is provided by protein motions, the major energy barrier for binding of external ligands from the solvent originates from the dissociation energy of the internal ligand (Fig. 7).

Cyt *c* is a relatively rigid protein (35, 36) and does not contain a native ligand binding pocket or ligand access pathway; consistently, the CO escape yield of CO-binding cytochrome *c* variants is relatively low (17, 23, 47). Consequently, protein motions are expected to enhance the probability of CO escape. Our observation that significant barriers for ligand escape from the heme environment are also present in carboxymethylated cytochrome *c* (Fig. 6) therefore supports the general notion that they arise from movements of the protein moiety.

Some members of the globin family, including nonsymbiotic plant hemoglobins and mammalian neuroglobins and cytoglobins, are also 6-coordinate heme proteins that bind external ligands (52). The CO geminate recombination on the picosecond/nanosecond time scale is, at least in neuroglobin (53)[4] and cytoglobin,[5] less extensive than in the sensor proteins studied in the present work. In these globins, CO dynamics between intraprotein cavities have been studied with lower time resolution (>10 ns). The temperature dependence of the small recombination phases on the submicrosecond time scale (the extent of which appears to correlate with the presence of an internal heme ligand (54)) also indicates virtually barrierless recombination toward the heme pocket and activated migration toward the solvent (55, 56), with barriers on the same order of magnitude as found in the present work. Thus, whereas these studies do not cover the initial ligand migration steps, comparison with our work supports that these properties are general features of 6-coordinate heme proteins.

In summary, our results provide evidence that the rearrangement motions of the intrinsic distal heme ligand (an amino acid residue) are largely responsible for the enthalpy barriers of the initial ligand escape pathway in 6-coordinate heme proteins. Ligand rebinding from the initial docking site is near barrierless. These findings are schematically represented in Fig. 7. For DNR, we have demonstrated NO-specific DNA binding and NO-heme dynamic interactions, typical for NO sensor proteins, which have potential to further unravel how these events at an ultrafast time scale eventually trigger chromatin recruitment. Mechanistic studies on the intraprotein signaling mechanism in DNR will be possible on a more detailed level when precise structural information on the heme binding properties is available.

Acknowledgment—We thank Dr. Hannu Myllykallio for critical reading of the manuscript.

REFERENCES

1. Germani, F., Moens, L., and Dewilde, S. (2013) Haem-based sensors: a still growing old superfamily in *Advances in Microbial Physiology* (Poole, R. K., ed) Vol. 63, pp. 1–47, Academic Press, Waltham, Massachusetts
2. Aono, S. (2012) Novel bacterial gas sensor proteins with transition metal-containing prosthetic groups as active sites. *Antioxid. Redox. Signal.* **16,** 678–686
3. Girvan, H. M., and Munro, A. W. (2013) Heme sensor proteins. *J. Biol. Chem.* **288,** 13194–13203
4. Arai, H., Igarashi, Y., and Kodama, T. (1995) Expression of the nir and nor genes for denitrification of *Pseudomonas aeruginosa* requires a novel CRP/FNR-related transcriptional regulator, DNR, in addition to ANR. *FEBS Lett.* **371,** 73–76
5. Castiglione, N., Rinaldo, S., Giardina, G., and Cutruzzolà, F. (2009) The transcription factor DNR from *Pseudomonas aeruginosa* specifically requires nitric oxide and haem for the activation of a target promoter in *Escherichia coli*. *Microbiology* **155,** 2838–2844
6. Giardina, G., Rinaldo, S., Johnson, K. A., Di Matteo, A., Brunori, M., and Cutruzzolà, F. (2008) NO sensing in *Pseudomonas aeruginosa*: structure of the transcriptional regulator DNR. *J. Mol. Biol.* **378,** 1002–1015
7. Lanzilotta, W. N., Schuller, D. J., Thorsteinsson, M. V., Kerby, R. L., Roberts, G. P., and Poulos, T. L. (2000) Structure of the CO sensing transcription activator CooA. *Nat. Struct. Biol.* **7,** 876–880
8. Roberts, G. P., Kerby, R. L., Youn, H., and Conrad, M. (2005) CooA, a paradigm for gas sensing regulatory proteins. *J. Inorg. Biochem.* **99,** 280–292
9. Borjigin, M., Li, H., Lanz, N. D., Kerby, R. L., Roberts, G. P., and Poulos, T. L. (2007) Structure-based hypothesis on the activation of the CO-sensing transcription factor CooA. *Acta Crystallogr. D Biol. Crystallogr.* **63,** 282–287
10. Liebl, U., Lambry, J. C., and Vos, M. H. (2013) Primary processes in heme-based sensor proteins. *Biochim. Biophys. Acta* **1834,** 1684–1692
11. Giardina, G., Rinaldo, S., Castiglione, N., Caruso, M., and Cutruzzolà, F. (2009) A dramatic conformational rearrangement is necessary for the activation of DNR from *Pseudomonas aeruginosa*. Crystal structure of wild-type DNR. *Proteins* **77,** 174–180
12. Stone, J. R., and Marletta, M. A. (1994) Soluble guanylate cyclase from bovine lung: activation with nitric oxide and carbon monoxide and spectral characterization of the ferrous and ferric states. *Biochemistry* **33,** 5636–5640
13. Vos, M. H. (2008) Ultrafast dynamics of ligands within heme proteins. *Biochim. Biophys. Acta* **1777,** 15–31
14. Liebl, U., Bouzhir-Sima, L., Kiger, L., Marden, M. C., Lambry, J. C., Négrerie, M., and Vos, M. H. (2003) Ligand binding dynamics to the heme domain of the oxygen sensor Dos from *Escherichia coli*. *Biochemistry* **42,** 6527–6535
15. Yamashita, T., Bouzhir-Sima, L., Lambry, J. C., Liebl, U., and Vos, M. H. (2008) Ligand dynamics and early signalling events in the heme domain of the sensor protein Dos from *Escherichia coli*. *J. Biol. Chem.* **283,** 2344–2352
16. Sousa, E. H., Tuckerman, J. R., Gonzalez, G., and Gilles-Gonzalez, M. A. (2007) DosT and DevS are oxygen-switched kinases in *Mycobacterium tuberculosis*. *Protein Sci.* **16,** 1708–1719
17. Silkstone, G., Jasaitis, A., Vos, M. H., and Wilson, M. T. (2005) Geminate carbon monoxide rebinding to a *c*-type haem. *Dalton Trans.* **21,** 3489–3494
18. Yamashita, T., Hoashi, Y., Watanabe, K., Tomisugi, Y., Ishikawa, Y., and Uno, T. (2004) Roles of heme axial ligands in the regulation of CO binding to CooA. *J. Biol. Chem.* **279,** 21394–21400

[4] L. Kiger and M. H. Vos, unpublished results.
[5] M. T. Wilson and M. H. Vos, unpublished results.

19. Vos, M. H., Bouzhir-Sima, L., Lambry, J. C., Luo, H., Eaton-Rye, J. J., Ioanoviciu, A., Ortiz de Montellano, P. R., and Liebl, U. (2012) Ultrafast ligand dynamics in the heme-based GAF sensor domains of the histidine kinases DosS and DosT from *Mycobacterium tuberculosis*. *Biochemistry* **51,** 159–166
20. Wilson, M. T., Brunori, M., Rotilio, G. C., and Antonini, E. (1973) Properties of modified cytochromes. II: Ligand binding to reduced carboxymethyl cytochrome *c*. *J. Biol. Chem.* **248,** 8162–8169
21. Creze, C., Ligabue, A., Laurent, S., Lestini, R., Laptenok, S. P., Khun, J., Vos, M. H., Czjzek, M., Myllykallio, H., and Flament, D. (2012) Modulation of the *Pyrococcus abyssi* NucS endonuclease activity by the replication clamp PCNA at functional and structural levels. *J. Biol. Chem.* **287,** 15648–15660
22. Thorsteinsson, M. V., Kerby, R. L., Conrad, M., Youn, H., Staples, C. R., Lanzilotta, W. N., Poulos, T. J., Serate, J., and Roberts, G. P. (2000) Characterization of variants altered at the N-terminal proline, a novel heme-axial ligand in CooA, the CO-sensing transcriptional activator. *J. Biol. Chem.* **275,** 39332–39338
23. Silkstone, G., Jasaitis, A., Wilson, M. T., and Vos, M. H. (2007) Ligand dynamics in an electron-transfer protein: picosecond geminate recombination of carbon monoxide to heme in mutant forms of cytochrome *c*. *J. Biol. Chem.* **282,** 1638–1649
24. Lukacs, A., Eker, A. P., Byrdin, M., Villette, S., Pan, J., Brettel, K., and Vos, M. H. (2006) Role of the middle residue in the triple tryptophan electron transfer chain of DNA photolyase: ultrafast spectroscopy of a Trp→Phe mutant. *J. Phys. Chem. B* **110,** 15654–15658
25. Snellenburg, J. J., Laptenok, S. P., Seger, R., Mullen, K. M., and van Stokkum, I. H. M. (2012) Glotaran: a Java-based graphical user interface for the R package TIMP. *J. Stat. Software* **49,** 1–22
26. Négrerie, M., Bouzhir, L., Martin, J. L., and Liebl, U. (2001) Control of nitric oxide dynamics by guanylate cyclase in its activated state. *J. Biol. Chem.* **276,** 46815–46821
27. Silkstone, G., Kapetanaki, S. M., Husu, I., Vos, M. H., and Wilson, M. T. (2010) Nitric Oxide binds to the proximal heme coordination site of the ferrocytochrome c / cardiolipin complex: formation mechanism and dynamics. *J. Biol. Chem.* **285,** 19785–19792
28. Kruglik, S. G., Lambry, J. C., Cianetti, S., Martin, J. L., Eady, R. R., Andrew, C. R., and Negrerie, M. (2007) Molecular basis for nitric oxide dynamics and affinity with *Alcaligenes xylosoxidans* cytochrome *c*. *J. Biol. Chem.* **282,** 5053–5062
29. Benabbas, A., Karunakaran, V., Youn, H., Poulos, T. L., and Champion, P. M. (2012) Effect of DNA binding on geminate CO recombination kinetics in CO-sensing transcription factor CooA. *J. Biol. Chem.* **287,** 21729–21740
30. Kumazaki, S., Nakajima, H., Sakaguchi, T., Nakagawa, E., Shinohara, H., Yoshihara, K., and Aono, S. (2000) Dissociation and recombination between ligands and heme in a CO-sensing transcriptional activator CooA. *J. Biol. Chem.* **275,** 38378–38383
31. Morris, R. J., and Gibson, Q. H. (1980) The role of diffusion in limiting the rate of ligand binding to hemoglobin. *J. Biol. Chem.* **255,** 8050–8053
32. Sardiwal, S., Kendall, S. L., Movahedzadeh, F., Rison, S. C., Stoker, N. G., and Djordjevic, S. (2005) A GAF domain in the hypoxia/NO-inducible *Mycobacterium tuberculosis* DosS protein binds haem. *J. Mol. Biol.* **353,** 929–936
33. Podust, L. M., Ioanoviciu, A., and Ortiz de Montellano, P. R. (2008) 2.3 Å x-ray structure of the heme-bound GAF domain of sensory histidine kinase DosT of *Mycobacterium tuberculosis*. *Biochemistry* **47,** 12523–12531
34. Petrich, J. W., Poyart, C., and Martin, J. L. (1988) Photophysics and reactivity of heme proteins: a femtosecond absorption study of hemoglobin, myoglobin and protoheme. *Biochemistry* **27,** 4049–4060
35. Flynn, P. F., Bieber Urbauer, R. J., Zhang, H., Lee, A. L., and Wand, A. J. (2001) Main chain and side chain dynamics of a heme protein: ^{15}N and ^{2}H NMR relaxation studies of *R. capsulatus* ferrocytochrome c_2. *Biochemistry* **40,** 6559–6569
36. Louie, G. V., and Brayer, G. D. (1990) High-resolution refinement of yeast iso-1-cytochrome *c* and comparisons with other eukaryotic cytochromes *c*. *J. Mol. Biol.* **214,** 527–555
37. Bren, K. L., and Gray, H. B. (1993) Structurally engineered cytochromes with novel ligand-binding sites: oxy and carbon monoxy derivatives of semisynthetic horse heart Ala80 cytochrome *c*. *J. Am. Chem. Soc.* **115,** 10382–10383
38. Brzezinski, P., and Wilson, M. T. (1997) Photochemical electron injection into redox-active proteins. *Proc. Natl. Acad. Sci. U.S.A.* **94,** 6176–6179
39. Larsen, R. W. (2003) Ligand binding subsequent to CO photolysis of methionine-modified cytochrome *c*. *Biochim. Biophys. Acta* **1619,** 15–22
40. Silkstone, G., Stanway, G., Brzezinski, P., and Wilson, M. T. (2002) Production and characterisation of Met80X mutants of yeast iso-1-cytochrome *c*: spectral, photochemical and binding studies on the ferrous derivatives. *Biophys. Chem.* **98,** 65–77
41. Kapetanaki, S. M., Silkstone, G., Husu, I., Liebl, U., Wilson, M. T., and Vos, M. H. (2009) Interaction of carbon monoxide with the apoptosis-inducing cytochrome *c*-cardiolipin complex. *Biochemistry* **48,** 1613–1619
42. Heyduk, T., and Lee, J. C. (1990) Application of fluorescence energy transfer and polarization to monitor *Escherichia coli* cAMP receptor protein and lac promoter interaction. *Proc. Natl. Acad. Sci. U.S.A.* **87,** 1744–1748
43. Yoo, B. K., Lamarre, I., Martin, J. L., and Negrerie, M. (2012) Quaternary structure controls ligand dynamics in soluble guanylate cyclase. *J. Biol. Chem.* **287,** 6851–6859
44. Lawson, D. M., Stevenson, C. E., Andrew, C. R., and Eady, R. R. (2000) Unprecedented proximal binding of nitric oxide to heme: implications for guanylate cyclase. *EMBO J.* **19,** 5661–5671
45. Martin, E., Berka, V., Sharina, I., and Tsai, A. L. (2012) Mechanism of binding of NO to soluble guanylyl cyclase: implication for the second NO binding to the heme proximal site. *Biochemistry* **51,** 2737–2746
46. Rubtsov, I. V., Zhang, T., Nakajima, H., Aono, S., Rubtsov, G. I., Kumazaki, S., and Yoshihara, K. (2001) Conformational dynamics of the transcriptional regulator CooA protein studied by subpicosecond mid-infrared vibrational spectroscopy. *J. Am. Chem. Soc.* **123,** 10056–10062
47. Kim, J., Park, J., Lee, T., and Lim, M. (2009) Dynamics of ultrafast rebinding of CO to carboxymethyl cytochrome *c*. *J. Phys. Chem. B* **113,** 260–266
48. Gonzalez, G., Dioum, E. M., Bertolucci, C. M., Tomita, T., Ikeda-Saito, M., Cheesman, M. R., Watmough, N. J., and Gilles-Gonzalez, M. A. (2002) Nature of the displaceable heme-axial residue in the *Ec*Dos protein, a heme-based sensor from *Escherichia coli*. *Biochemistry* **41,** 8414–8421
49. Rinaldo, S., Castiglione, N., Giardina, G., Caruso, M., Arcovito, A., Longa, S. D., D'Angelo, P., and Cutruzzolà, F. (2012) Unusual heme binding properties of the dissimilative nitrate respiration regulator, a bacterial nitric oxide sensor. *Antioxid. Redox Signal.* **17,** 1178–1189
50. Liebl, U., Bouzhir-Sima, L., Negrerie, M., Martin, J. L., and Vos, M. H. (2002) Ultrafast ligand rebinding in the heme domain of the oxygen sensors FixL and Dos: general regulatory implications for heme-based sensors. *Proc. Natl. Acad. Sci. U.S.A.* **99,** 12771–12776
51. Puranik, M., Nielsen, S. B., Youn, H., Hvitved, A. N., Bourassa, J. L., Case, M. A., Tengroth, C., Balakrishnan, G., Thorsteinsson, M. V., Groves, J. T., McLendon, G. L., Roberts, G. P., Olson, J. S., and Spiro, T. G. (2004) Dynamics of carbon monoxide binding to CooA. *J. Biol. Chem.* **279,** 21096–21108
52. Kakar, S., Hoffman, F. G., Storz, J. F., Fabian, M., and Hargrove, M. S. (2010) Structure and reactivity of hexacoordinate hemoglobins. *Biophys. Chem.* **152,** 1–14
53. Nienhaus, K., Kriegl, J. M., and Nienhaus, G. U. (2004) Structural dynamics in the active site of murine neuroglobin and its effects on ligand binding. *J. Biol. Chem.* **279,** 22944–22952
54. Bruno, S., Faggiano, S., Spyrakis, F., Mozzarelli, A., Abbruzzetti, S., Grandi, E., Viappiani, C., Feis, A., Mackowiak, S., Smulevich, G., Cacciatori, E., and Dominici, P. (2007) The reactivity with CO of AHb1 and AHb2 from *Arabidopsis thaliana* is controlled by the distal HisE7 and internal hydrophobic cavities. *J. Am. Chem. Soc.* **129,** 2880–2889
55. Bisht, N. K., Abbruzzetti, S., Uppal, S., Bruno, S., Spyrakis, F., Mozzarelli, A., Viappiani, C., and Kundu, S. (2011) Ligand migration and hexacoordination in type 1 non-symbiotic rice hemoglobin. *Biochim. Biophys. Acta* **1814,** 1042–1053
56. Gabba, M., Abbruzzetti, S., Spyrakis, F., Forti, F., Bruno, S., Mozzarelli, A., Luque, F. J., Viappiani, C., Cozzini, P., Nardini, M., Germani, F., Bolognesi, M., Moens, L., and Dewilde, S. (2013) CO rebinding kinetics and molecular dynamics simulations highlight dynamic regulation of internal cavities in human cytoglobin. *PLoS One* **8,** e49770